Draft version April 18, 2020
Preprint typeset using LaTeX style emulateapj v. 12/16/11

MEASURING GRAVITATIONAL-WAVE HIGHER-ORDER MODES

J. C. Mills, S. Fairhurst
School of Physics and Astronomy, Cardiff University, The Parade, Cardiff, CF24 3AA, UK
Draft version April 18, 2020

ABSTRACT

We investigate the observability of higher harmonics in gravitational wave signals emitted during the coalescence of binary black holes. We decompose each mode into an overall amplitude, dependent upon the masses and spins of the system, and an orientation-dependent term, dependent upon the inclination and polarization of the source. Using this decomposition, we investigate the significance of higher modes over the parameter space and show that the 33 mode is most significant across much of the sensitive band of ground-based interferometric detectors, with the 44 having a significant contribution at high masses. Next, we introduce the signal-to-noise ratio in each higher mode as, e.g. ρ_{33}, and argue that an observed higher mode SNR > 2.1 is unlikely to occur due to noise alone.

1. INTRODUCTION

Gravitational waves emitted during the coalescence of black hole and/or neutron star binaries are well known to emit predominantly at twice the orbital frequency, during the inspiral phase of the coalescence. However, it is also well-known that the gravitational wave signal cannot be completely characterized by a single harmonic but, rather, is better decomposed as a sum of spin-weighed spherical (or spheroidal) harmonics. The dominant harmonic is the $\ell = 2$, $m = \pm 2$ harmonic, but there is also power in higher harmonics, most notably the 21, 33 and 44 harmonics. The importance of these additional harmonics increases as the mass ratio between the two black holes increases and also increases during the late inspiral and merger of the objects. Recent semi-analytical and numerical relativity models have provided expressions for an increasing number of the higher harmonics accurate across the inspiral, merger and ringdown regimes Mehta et al. (2017); London et al. (2018); Khan et al. (2019); Khan et al. (2020); Kumar Mehta et al. (2019); Cotesta et al. (2018); Varma et al. (2019b,a); Rifat et al. (2019); Nagar et al. (2020); Garca-Quirs et al. (2020); Cotesta et al. (2020); Ossokine et al. (2020).

The observation of higher gravitational-wave harmonics from a binary merger is interesting for several reasons. Firstly, it provides further evidence that Einstein's general relativity is an accurate description of gravity, including in the strong-field, highly dynamic regime of the merger of two black holes. Second, by incorporating knowledge of the higher harmonics into a search for gravitational waves, the sensitivity of the search could be increased, leading to an increase in the rate of observed systems Harry et al. (2018); furthermore these systems would typically be from interesting parts of the parameter space, for example with high mass ratios. Third, the observation of the higher harmonics enables more accurate measurement of the properties of system Kalaghatgi et al. (2019). For example, the measurement of multiple harmonics can be used to break well-known degeneracies between the measured distance and orientation of the system, or the mass ratio and spins of the black holes.

While the gravitational waveform is comprised of contributions from an infinite number of harmonics, it is really the unambiguous measurement of a *second harmonic* (in addition to the 22-harmonic) which will lead to a step-change in our ability to measure the properties of the system; additional harmonics will then further refine the measurement accuracy. Consequently, in this paper, we perform an in-depth investigation of the importance of the higher harmonics across the parameter space and identify those which are likely to make the most significant contribution. The amplitude of each harmonic depends both upon the intrinsic parameters of the system (its masses and spins, both magnitudes and orientations) as well as the extrinsic parameters (the orientation of the binary and the detector network's sensitivity to the two polarizations of gravitational waves). For simplicity, we decompose the harmonics into an overall amplitude factor, dependent only upon the extrinsic parameters, and an orientation dependent term. We then investigate the significance of each harmonic across the parameter space.

Next, we turn to the question of *when* additional harmonics have been unambiguously observed. From a model selection perspective, this can be addressed by considering the evidence in favour of a waveform containing higher harmonics against one without. Here, we introduce the higher-harmonic signal to noise ratio, and argue that this can be used as an alternative method of establishing the observability of higher harmonics. A similar prescription has recently been introduced for precessing systems Fairhurst et al. (2019a,b). It is straightforward to obtain the SNR contained in each of the waveform harmonics (with the higher harmonics appropriately orthogonalized so as not to pick up any power from the dominant harmonic). In principle, the waveform parameters can all be measured from the dominant harmonic. However, due to limited SNR and well-known degeneracies between parameters Usman et al. (2019), it is often the case that the observation of only the 22-harmonic provides little information about the expected higher mode signal. Consequently, we argue that, in many cases, the amplitude and phase of the second most significant mode are essentially unconstrained. This allows us to infer the expected distribution in the presence of noise alone and to propose a straightforward threshold on power in the second most significant harmonic as a simple criterion for the observation of higher harmonics in a gravitational wave signal.

2. WAVEFORM

The measured gravitational wave strain h can be written as

$$h = F_+(\alpha_s, \delta_s, \chi)h_+ + F_\times(\alpha_s, \delta_s, \chi)h_\times. \tag{1}$$

Where α_s, δ_s denote the right-ascension and declination of the source. The antenna factors $F_+(\alpha_s, \delta_s, \chi)$ and $F_\times(\alpha_s, \delta_s, \chi)$ relate the polarizations h_+ and $h_\times$ in the radiation-frame to the detector-frame. We define $F_+(\alpha_s, \delta_s, \chi)$ and $F_\times(\alpha_s, \delta_s, \chi)$ in the dominant polarization frame Klimenko et al. (2005); Harry & Fairhurst (2011), which for each sky point the polarization angle χ is chosen to maximize the network sensitivity to F_+. This gives us a sense to what extent a network is sensitive to two independent polarizations for a given sky point. We have this freedom of choice for χ by leaving free a further polarization angle ψ. A counter-clockwise rotation by ψ transforms h'_+ and $h'_\times$ as

$$\begin{aligned} h_+ =& h'_+ \cos 2\psi + h'_\times \sin 2\psi \\ h_\times =& - h'_+ \sin 2\psi + h'_\times \cos 2\psi \,. \end{aligned} \tag{2}$$

Since the observed strain depends only upon the sum of the two angles ψ and χ, we are free to fix one of them to a convenient value; we utilise this freedom to work in the dominant polarization basis. The radiation-frame gravitational polarizations h'_+ and $h'_\times$ can be decomposed into modes using spin-weighted spherical harmonics of spin weight -2, ${}_{-2}Y_{lm}$, which depend on the inclination angle ι and coalescence phase ϕ_c, as [1]

$$h'_+ - ih'_\times = \sum_{l\geq 2}\sum_{m=-l}^{l} {}_{-2}Y_{lm}(\iota, \phi_c)h_{lm} \tag{3}$$

For a binary merger which does not exhibit precession, the waveform can be expressed in the frequency domain, using the stationary-phase approximation, as

$$\begin{aligned} h_+ &= \frac{1}{2}\sum_{l\geq 2}\sum_{m=1}^{l} A_+^{lm}\tilde{h}_{lm}(f) \\ h_\times &= \frac{i}{2}\sum_{l\geq 2}\sum_{m=1}^{l} A_\times^{lm}\tilde{h}_{lm}(f) \end{aligned} \tag{4}$$

where

$$\begin{aligned} A_+^{lm} &= \left[{}_{-2}Y_{lm}(\iota, \phi_c) + (-1)^l {}_{-2}Y^*_{l-m}(\iota, \phi_c)\right] \\ A_\times^{lm} &= \left[{}_{-2}Y_{lm}(\iota, \phi_c) - (-1)^l {}_{-2}Y^*_{l-m}(\iota, \phi_c)\right] \end{aligned} \tag{5}$$

See Appendix A for a more detailed discussion of the decomposition.

Using these expressions it is straightforward to derive the dependence of each multipole upon the binary inclination ι. The dependence for the most significant harmonics is

$$\begin{aligned} A_+^{22} &= \tfrac{1}{2}(1+\cos^2\iota) \\ A_\times^{22} &= \cos\iota \\ A_+^{21} &= \sin\iota \\ A_\times^{21} &= \sin\iota\cos\iota \\ A_+^{33} &= \sin\iota(1+\cos^2\iota) \\ A_\times^{33} &= 2\sin\iota\cos\iota \\ A_+^{32} &= 1-2\cos^2\iota \\ A_\times^{32} &= \tfrac{1}{2}(\cos\iota - 3\cos^3\iota) \\ A_+^{44} &= \sin^2\iota(1+\cos^2\iota) \\ A_\times^{44} &= 2\sin^2\iota\cos\iota \end{aligned} \tag{6}$$

and each mode will have an $e^{im\phi_c}$ dependence on the phase angle. For the 22 mode, it is customary to choose a normalization such that $A_+^{22} = A_\times^{22} = 1$ for a face-on system, and we use that normalization here. Since many of the higher harmonics vanish for face-on systems, we instead choose a normalization for the higher-mode amplitudes, $A_{+,\times}^{lm}$ in Eq. (6), by requiring that the plus polarization A_+^{lm} is unity for $\iota = \frac{\pi}{2}$, i.e. when the system is edge on. Figure 1 shows the dependence of the modes on inclination. The plus polarization of the 22 mode peaks at face-on, while the 21 and 44 modes peak at edge-on. The 32 mode is maximum at both face-on and edge-on orientations while the 33 mode hand peaks at $\sin\iota = \sqrt{\frac{2}{3}}$.

During inspiral the frequency evolution of a multipole ω_{lm}, is related to the orbital frequency ω_{orb} as $\omega_{lm} \sim m\omega_{orb}$. While during the ringdown the frequency approximately evolves as $\omega_{lm} \sim l\omega_{orb}$. Thus it is possible to scale the frequencies of the 22 mode in quite a simple manner to obtain an approximate phase evolution of the $l = m$ harmonics, for example the phase evolution of the 33 mode is a factor of 1.5 times ω_{22}.

3. OBSERVABILITY

The gravitational wave signal from every binary merger will be comprised of the sum of an infinite number of harmonics. However, for the majority of signals observed close to threshold, only the dominant 22 harmonic will be observable above the noise background. In this section, we investigate the observability of the different modes, and how this varies across the mass and spin parameter space. For concreteness, we restrict attention to a single detector with a sensitivity comparable to that achieved by the LIGO observatories during their third observing run. The power spectral density for the analysis is given in Appendix B Abbott et al. (2016).

The key metric for waveform observability is the optimal signal-to-noise ratio (SNR) defined as

$$\rho = \sqrt{(h|h)}\,, \tag{7}$$

where we have introduced the inner product weighted by noise characterized by a power spectrum $S(f)$

$$(a|b) := 4\,\mathrm{Re}\int_0^{f_{\max}} \frac{\tilde{a}(f)\tilde{b}(f)^\star}{S(f)}\,\mathrm{d}f\,. \tag{8}$$

[1] See Appendix A for a more detailed discussion of the decomposition.

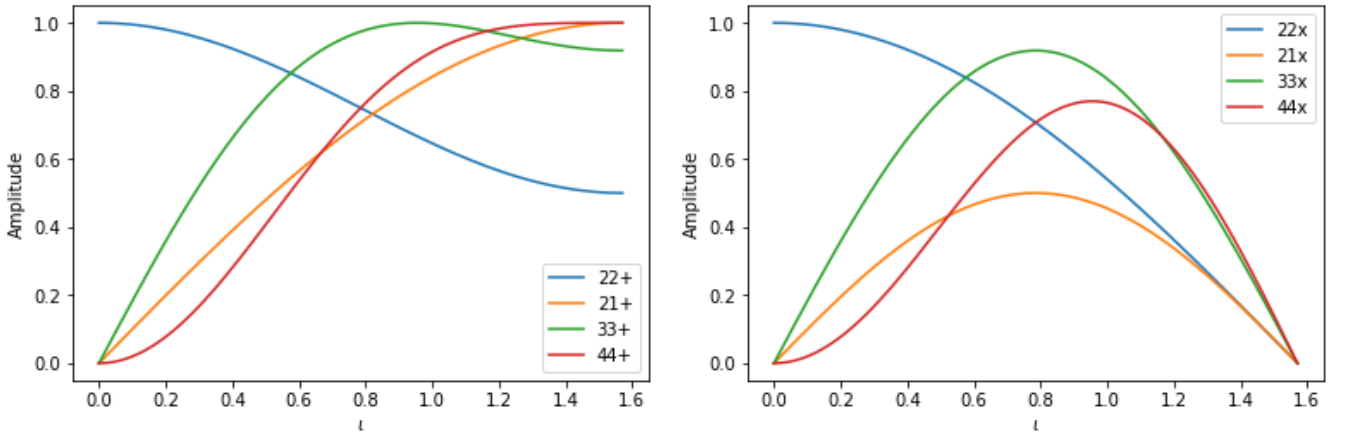

Figure 1. Dependence on the inclination angle of each mode.

Consider the situation where the 22 mode has been observed, and we are interested in obtaining an estimate of the expected SNR in the other harmonics. As is clear from Eq. (4), the SNR in the higher harmonics will depend upon the detector sensitivity to the higher harmonic waveform, $\tilde{h}_{\ell m}$, as well as the amplitude factor $A^{\ell m}_{+,\times}$. The sensitivity of the detector to a given harmonic is encoded by

$$\sigma_{\ell m} = \sqrt{(\tilde{h}_{\ell m}|\tilde{h}_{\ell m})}\,. \tag{9}$$

The amplitude of each multipole depends on both the intrinsic properties of the system and the orientation relative to the network of detectors. We are interested in quantifying the contribution of higher multipoles to a signal relative to the dominant. For simplicity we first consider just two multipoles: $\ell m = (2,2)$ and $\ell m = (3,3)$. From (1), (4) and (7), the waveform in detector i is given by

$$h_i = h_i^{22} + h_i^{33} = F_+^i(h_+^{22} + h_+^{33}) + F_\times^i(h_\times^{22} + h_\times^{33}) \tag{10}$$

In the dominant polarization frame $F_\times \cdot F_+ = 0$ so we can write the network optimal SNR as

$$\begin{aligned}\rho^2 =& F_+^2\left[|h_+^{22}|^2 + |h_+^{33}|^2 + 2(h_+^{33}|h_+^{22})\right] \\ &+F_\times^2\left[|h_\times^{22}|^2 + |h_\times^{33}|^2 + 2(h_\times^{33}|h_\times^{22})\right]\end{aligned} \tag{11}$$

The cross terms such as $(h_+^{33}|h_+^{22})$ can be both positive or negative, causing constructive or destructive interference between the harmonics. As discussed previously, the frequency during inspiral scales with ℓ while the ringdown frequency scales approximately with m. Consequently, there is typically little overlap between the 22 mode and modes for which both $\ell \neq 2$ and $m \neq 2$. Since the loudest subdominant multipoles are usually $\ell m = (3,3)$ and $\ell m = (4,4)$ we neglect these cross terms for now, but will revisit their significance later. Doing this allows us to write

$$\begin{aligned}\rho^2 =& F_+^2|h_+^{22}|^2\left[1 + \frac{|h_+^{33}|^2}{|h_+^{22}|^2}\right] \\ &+F_\times^2|h_\times^{22}|^2\left[1 + \frac{|h_\times^{33}|^2}{|h_\times^{22}|^2}\right]\,.\end{aligned} \tag{12}$$

The cross and plus polarizations for multipoles with $\ell = m$ are obtained by multiplying the 22 polarizations by the same overall factors, $\sin^{(\ell-2)}\iota$. Therefore $\frac{|h_+^{33}|^2}{|h_+^{22}|^2} = \frac{|h_\times^{33}|^2}{|h_\times^{22}|^2}$. To make this explicit we factor out the dependence of inclination and compute the ratio at fiducial inclinations such that $A^+_{lm} = 1$ (i.e. 0 for the 22 multipole and $\pi/2$ for higher multipoles). Thus we define the ratio at these fiducial inclinations as

$$\alpha_{\ell m} = \frac{\sigma_{\ell m}}{\sigma_{22}}\,, \tag{13}$$

We can thus write the SNR, ignoring the cross terms, as

$$\rho^2 = \rho_{22}^2 + \rho_{\ell m}^2\,, \tag{14}$$

where

$$\rho_{\ell m} = \rho_{22}\alpha_{\ell m}R_{\ell m} \tag{15}$$

and

$$\begin{aligned}R_{33}(\iota) &= 2\sin\iota \\ R_{44}(\iota) &= 2\sin^2\iota\,.\end{aligned} \tag{16}$$

The factor of two in (16) arises because the 22 mode amplitude $A^{22}_{+,\times}$ is half of the other modes at $\iota = \frac{\pi}{2}$. For other modes, the relative SNRs can be expressed in a similar manner but now the geometric factor R will depend also upon the polarization angle ψ.

3.1. *Extrinsic parameters*

As discussed previously, we are interested in understanding the expected power in higher harmonics, given the observation of the 22 mode. From the form of Eq. (16), we note two things immediately: it is possible that there is zero amplitude for both the 33 and 44 harmonics, and this occurs when the system is face on ($\iota = 0$); the maximum value of the geometric factor is two, and this occurs when the system is edge on ($\iota = \frac{\pi}{2}$). Next, we consider the distribution of R for a population of sources distributed uniformly in volume[2] and with uniformly distributed orientation. In figure 2 we plot the

[2] Realistically, we do not expect sources to be uniformly distributed, due to both cosmological effects and a redshift dependent rate Madau & Dickinson (2014). Nonetheless, this simple model provides a reasonably approximation to gain an understanding of the likely values of R.

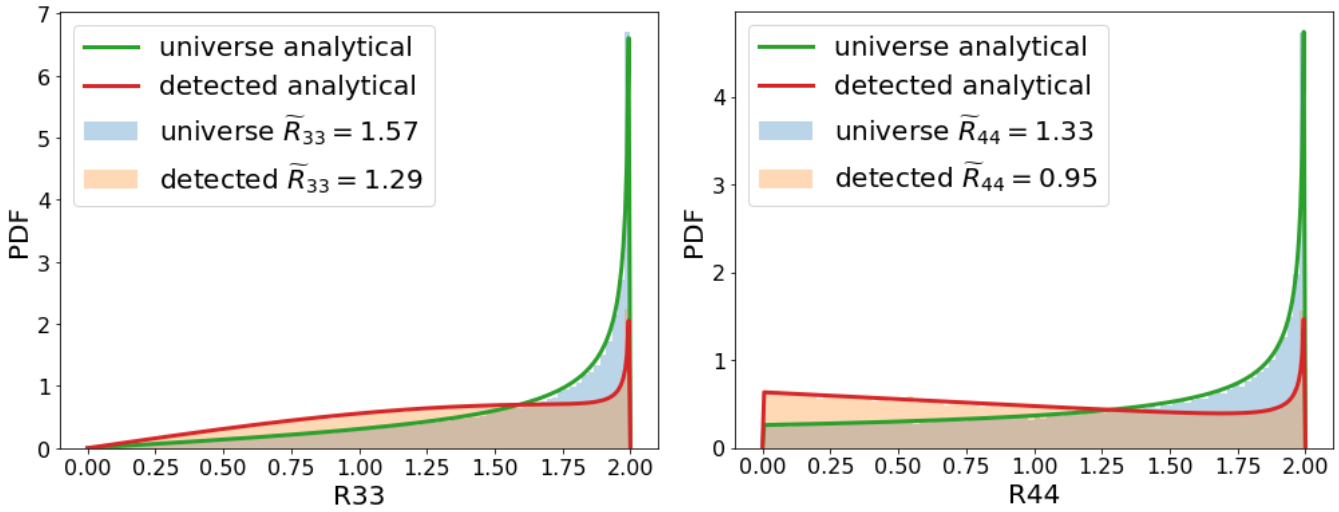

Figure 2. Distribution of $R_{33}(\iota)$ and $R_{44}(\iota)$ for all binaries (Universe) as well as that subset that would be detected above a fixed SNR threshold for the 22 harmonic (Detected). We show both the results from a Monte-Carlo simulation as well as the analytical prediction.

expected distribution of the geometrical factors $R_{33}(\iota)$ and $R_{44}(\iota)$. We show both the distribution based upon uniformly distributed sources, as well as the expected observed distribution – obtained by placing a threshold upon the observed SNR in the dominant 22 harmonic Schutz (2011). In both cases, for both the 33 and 44 harmonic, the distribution peaks at $R = 2$, the value for an edge-on system. However, selection effects serve to significantly reduce the peak, as this is the orientation that gives the least power in the 22 harmonic.

For other modes, the expected distribution of $R_{\ell m}$ will depend upon the sensitivity of the detector network to the two polarizations of the gravitational wave — the distribution for $R_{\ell m}$ will differ between a single detector, sensitive to only one polarization, and a network with good sensitivity to both polarizations. Nonetheless, the distribution for R_{21} will share features with R_{33} and R_{44}, namely it will take values between 0 (face on) and 2 (edge on), with a peak at $R_{21} = 2$ which is reduced by selection effects in the observed population. $R_{32} \lesssim 1$ for sources near to face-on, and so there is a significant contribution there as well as at the maximum of $R_{32} = 2$ which occurs for edge-on systems.

3.2. *Relative strength of higher modes*

The two important intrinsic parameters determining the relative power in the higher modes are mass ratio and total mass, with spin effects entering at higher post-Newtonian (PN) order for most modes (Mishra et al. 2016). The contribution of a higher mode relative to the dominant 22 mode increases with an increasing mass ratio. The relative amplitudes of the modes is independent of the total mass of the system. However the frequency content of each mode is does depend upon the total mass and thus depending on the shape of the detector PSD certain higher modes might be preferentially observed.

In Fig 3 we show the relative amplitude α_{lm} in the 33 and 44 multipoles, calculated using the waveform approximant PhenomHM London et al. (2018), for a signal observed in a detector with LIGO O3 sensitivity, as a function of the total mass and mass ratio of the system. Generally, the 33 mode will be the loudest subdominant mode. For symmetric mass binaries, and particularly those with large masses, the 44 mode will be the loudest.

Now, for the power in these modes to be observable, it must be possible to distinguish the mode from the 22 harmonic. Generally, it is only the contribution which is *orthogonal* to the 22 harmonic which will be observable. Any contribution from the higher harmonics which is proportional to the 22 harmonic will simply serve to change the power observed in the 22. Consequently, we are interested in knowing whether the waveforms are orthogonal or, equivalently, what the overlap between the modes is. Here, we define the normalized overlap maximized over ϕ_c

$$O(\ell m, 22) = \frac{\mathrm{Max}_{\phi_c}(\tilde{h}_{\ell m}|\tilde{h}_{22})}{|\tilde{h}_{\ell m}||\tilde{h}_{22}|} \,. \tag{17}$$

The overlap between the 33 and 44 modes with the 22 harmonic is $< 10\%$ across the parameter space, as expected due to the fact that the frequency evolution of these harmonics differs significantly from the 22. Plots of overlaps of all multipoles can be seen in the supplementary material Mills & Fairhurst (2020).

Next, we turn our attention to the 32 and 21 harmonics. In figure 4 we show the amplitude of the 21 harmonic. The 21 mode is the only subdominant mode considered in this paper which has spin terms in the amplitude at 1 PN order Mishra et al. (2016). For this reason, the 21 mode can become more significant for binaries with large asymmetric spins, and consequently we show the relative mode amplitude for two different spins. Two facts determine the behaviour of α_{21} with increasing total mass. First α_{21} is largest at merger. Second the 21 merger is at a lower frequency than the 22. Initially α_{21} will increase with total mass as more of the merger is in the bucket. As the mass continues to increase, the 21 mode amplitude is no longer observable as it merges at too low a frequency, and so α_{21} decreases. Furthermore, the 21 multipole has the same frequency as the 22 mode during ringdown, and has a large overlap for ringdown-dominated signals, as shown in Fig 5.

In Figure 6, we show the significance of the 32 multi-

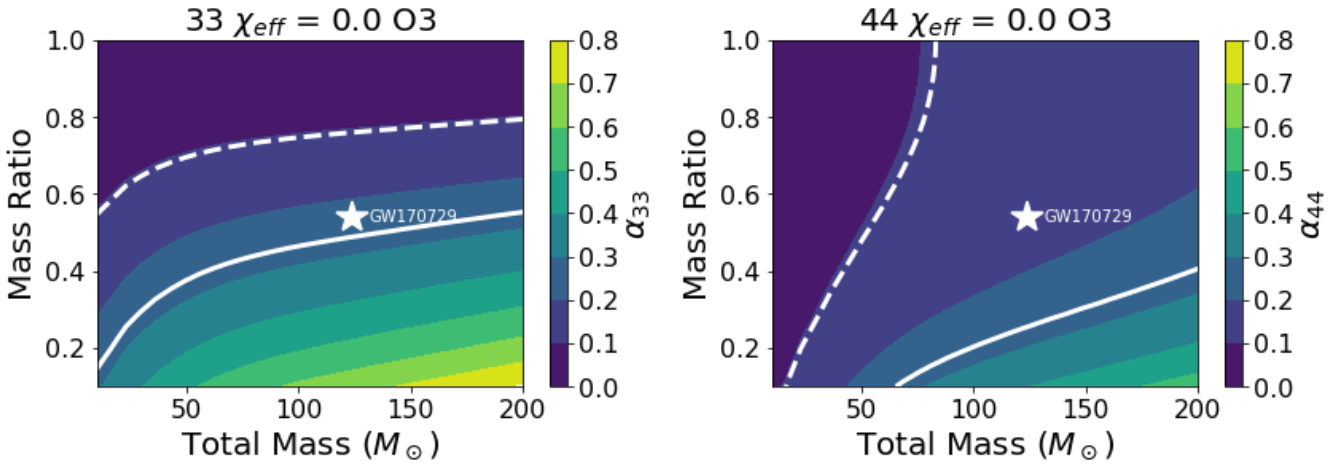

Figure 3. Ratio of the intrinsic amplitudes in Advanced LIGO (O3) of the $\ell, m = (3, 3)$ and $\ell, m = (4, 4)$ multipoles to the $\ell, m = (2, 2)$ multipole as a function of mass ratio and total mass ($M_\odot$). The figures show $\alpha_{\ell m}$ as defined in Eq. (13). For reference, we also mark the mass and mass ratio of GW170729, which was the first signal with some observable evidence for higher harmonics.

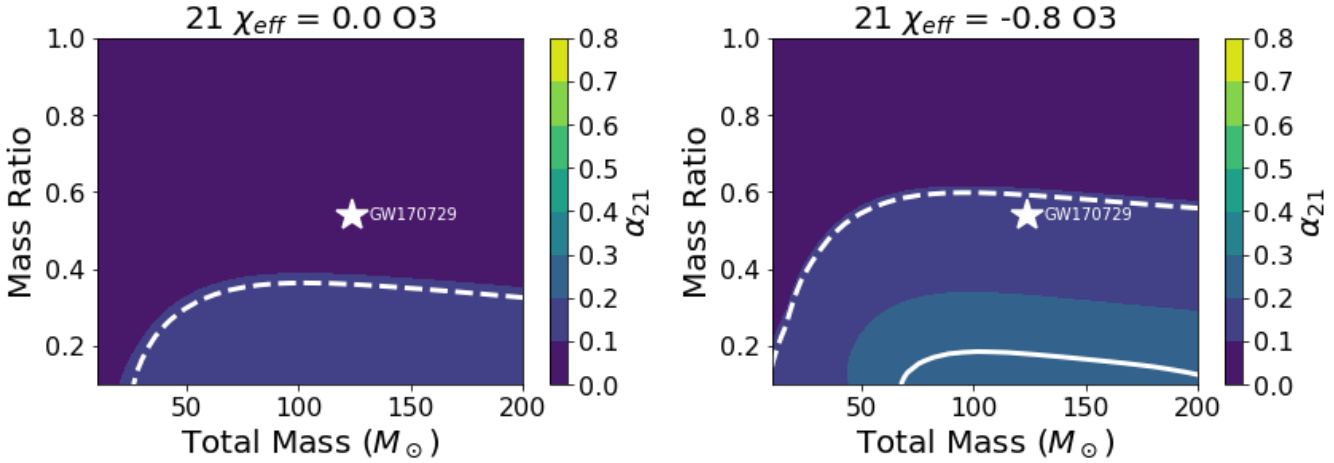

Figure 4. Ratio of the signal-to-noise ratio in Advanced LIGO (O3) of the $\ell, m = (2, 1)$ to the $\ell, m = (2, 2)$ multipole as a function of mass ratio and total mass ($M_\odot$) for an overhead system viewed edge-on with spins parallel to the orbital angular momentum: *Left:* $\chi_{\rm eff} = 0.0$, *Right:* $\chi_{\rm eff} = -0.8$. Plotted for a maximum value of α_{21} 0.8, to allow for easy comparison with other multipoles and detectors.

pole and its overlap with the 22 mode. Comparison with figure 3 shows that the 32 mode is generally less significant than either the 33 or 44 modes. In addition, there is significant overlap between the 22 and 32 modes, particularly for low masses. This is to be expected, as the 32 multipole oscillates at the same frequency as the 22 during the inspiral. Interestingly, one of the most significant impact of the 32 mode can be to produce an incorrect estimate of the amplitude of the 22 mode, and consequently introduce an error in the measured distance, as power from the 32 mode will be mistakenly attributed to the 22 mode.

Contribution of the other modes scales monotonically with increasing mass since the merger frequencies are higher than the 22. ET's sensitivity extends to lower frequency than aLIGO and it is thus sensitive to heavier binaries. The highest mass events might have a 22 merger-ringdown waveform that is cut off by the steeply rising noise floor of the detector at low frequencies. In addition to scaling the frequencies, mass also increases the amplitude of the gravitational wave. Therefore even in the absence of a detectable 22 waveform, subdominant modes which merge at higher frequencies might be observable. For this reason, studies quantifying the observability of such systems ought to include these modes.

4. MEASUREMENT

A simple way to quantify evidence for higher multipoles within a signal is to look at the results from parameter estimation. Do the inferred system properties correspond to waveforms with relatively large contributions from higher-order multipoles? For concreteness we will discuss results for the 33 multipole, which for most events will be the largest subdominant multipole. We calculate the component of the 33 optimal SNR that is orthogonal to the 22 multipole $\rho^{\perp}_{33}$ and so necessarily represents new evidence in the data.

$$\rho^{\perp}_{33} = \rho_{33}\sqrt{1 - O(33, 22)^2} \tag{18}$$

In Fig. 7 we show the inferred posterior probability distribution for $\rho^{\perp}_{33}$ for a binary with masses $m_1 = 40M_\odot$, $m_2 = 10M_\odot$ inclined at $\cos\iota = 0.7$ and with $\rho_2 2 = 20$ under a variety of assumptions for signal and model.

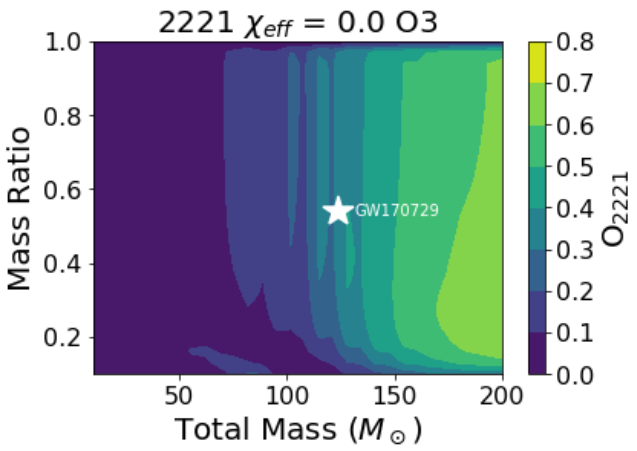

Figure 5. Absolute value of the noise-weighted inner product between the $\ell, m = (2, 2)$ the $\ell, m = (2, 1)$ multipole in Advanced LIGO (O3) as a function of mass ratio and total mass ($M_\odot$) for an overhead system viewed edge-on with spins parallel to the orbital angular momentum, $\chi_{\rm eff} = 0.0$. Plotted for a maximum value of O_{2221} 0.8, to allow for easy comparison with other multipoles and detectors.

Parameter estimates were obtained with LALInference Veitch et al. (2015). The green curve shows the distribution when a the 33 mode is present in both the signal and the waveform model. This peaks at $\rho_3 3^\perp \sim 5$ consistent with the injected SNR in the 33 mode. If instead the signal contained only the 22 multipole, the inferred distribution is very different. The blue, red, purple and brown curves are different noise realizations of this scenario. We see that most of the noise realizations correspond very closely to a χ-distribution with two degrees of freedom (the pink dashed line). The inferred distribution for first noise realization (red histogram) is peaked at a larger $\rho_3 3^\perp$, indicating an excess of gaussian noise in the 33 multipole filter.

In order to interpret these distributions, we calculate the expected distribution under some simplifying assumptions. Specifically, we consider the scenario where the 22 measurement has already fixed the parameters which determine the phase evolution of the binary (primarily the chirp mass, but also a combination of aligned spin and mass ratio). Typically however, the binary orientation and phase is not well measured. We show this in Fig. 8 which is the inferred probability distribution of inclination, distance, polarization and phase at coalescence posterior probability distributions for the above binary estimated with a waveform model containing only the dominant 22 multipole. The system is recovered as consistent with face-on and so, due to degeneracies Usman et al. (2019), the only well measured quantities are $A_{22} = \frac{\cos\iota}{D_L}$ and $\phi_{22} = \psi \pm \phi_c$. This means we still effectively have two degrees of freedom in the amplitude parameters. We are thus free to tune the amplitude and phase of the 33 multipole in order to best match the data. Another way to see this is to look at the posterior probabilty distribution for the 33 amplitude inferred when using a 22-only waveform model (see orange curve in Fig. 7). The distribution is broad and has support across a large range of ρ_{33}. The measurement thus has this as a prior and can produce more peaked posteriors within this range. Also shown in this plot is a distribution inferred for the 33 when no signal was injected. We can understand the shape of these distributions with a simplified model where the amplitude and phase of the 33 are free and the prior probability is uniform, which we have argued is a good approximation for the above system. Therefore we have a template

$$h = a h_0^{33} + b h_{\frac{\pi}{2}}^{33} + h_{22} \tag{19}$$

Where h_0^{33} and $h_{\frac{\pi}{2}}^{33}$ are the two phases of the waveform of the 33 waveform, a and b control the overall amplitude of these parameters, and h_{22} denotes all dominant mode contributions to the waveform. We assume the only free parameters are a and b, which determine the 33 amplitude and phase. In what follows we neglect constant terms such as h_{22} as we are interested in the form of the posterior probability distribution for a and b given a signal s, and uniform prior $\pi(a.b)$

$$p(a, b|s) \propto \Lambda(a, b)\pi(a, b)\,. \tag{20}$$

The likelihood of a signal s given the amplitudes a, b and gaussian noise is

$$\Lambda(s|a, b) \propto \exp\left[-\frac{1}{2}\left(s - h(a, b)|s - h(a, b)\right)\right]\,. \tag{21}$$

Using polar variables $\rho_{33} = \sqrt{a^2 + b^2}$ and $\phi_{33} = \arctan(b/a)$, and assuming a uniform prior we can write the posterior probability distribution for the amplitudes a and b given a signal s as

$$p(a, b|s)dadb \propto \Lambda(a, b)dadb \tag{22}$$

$$= \exp\left[a(s|h_0^{33}) + b(s|h_{\frac{\pi}{2}}^{33}) - \frac{a^2 + b^2}{2} - \frac{(s|s)}{2}\right] dadb \tag{23}$$

$$= \rho_{33} \exp\left[-\frac{\rho_{33}^2 + (s|s)}{2} + \rho_{33}\cos\phi_{33}(s|h_0^{33}) + \rho_{33}\sin\phi_{33}(s|h_{\frac{\pi}{2}}^{33})\right] d\rho_{33}d\phi_{33} \tag{24}$$

Defining the matched filter signal-to-noise ratio $\rho_{33}^{MF} = \sqrt{(s|h_0^{33})^2 + (s|h_{\frac{\pi}{2}}^{33})^2}$ and phase $\phi_{33}^{MF} = \arctan\frac{(s|h_{\frac{\pi}{2}}^{33})}{(s|h_0^{33})}$ and marginalizing over ϕ_{33}, we obtain

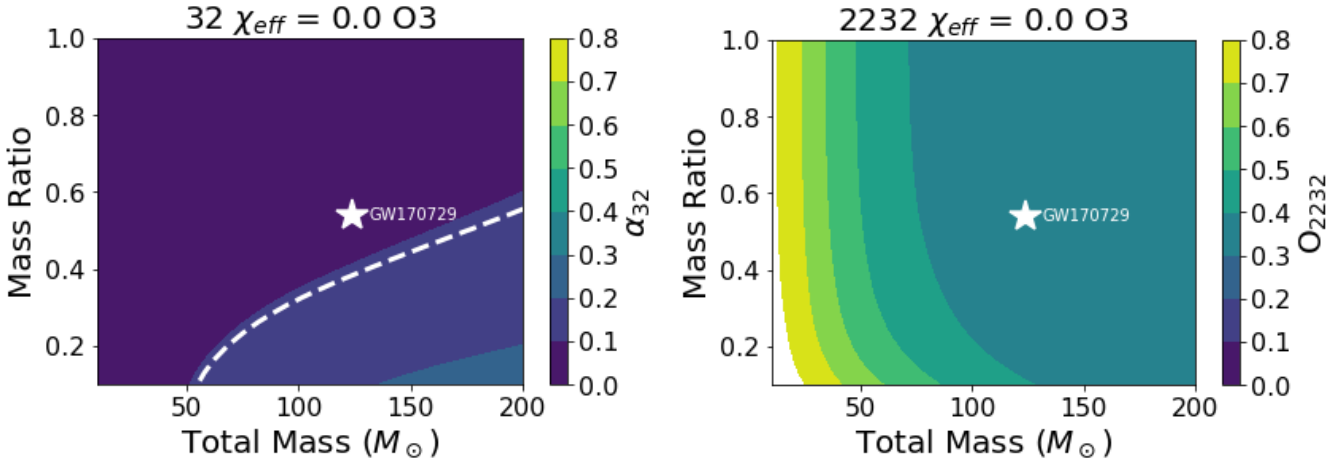

Figure 6. *Left:* Ratio of the signal-to-noise ratio in Advanced LIGO (O3) of the $\ell, m = (3, 2)$ to the $\ell, m = (2, 2)$ multipole as a function of mass ratio and total mass ($M_\odot$) for an overhead system viewed edge-on with spins parallel to the orbital angular momentum, $\chi_{\rm eff} = 0.0$. Plotted for a maximum value of α_{32} 0.8, to allow for easy comparison with other multipoles and detectors. *Right:* Absolute value of the noise-weighted inner product between the $\ell, m = (2, 2)$ the $\ell, m = (2, 2)$ multipole in Advanced LIGO (O3) as a function of mass ratio and total mass ($M_\odot$) for an overhead system viewed edge-on with spins parallel to the orbital angular momentum, $\chi_{\rm eff} = 0.0$. Plotted for a maximum value of O_{2232} 0.8, to allow for easy comparison with other multipoles and detectors.

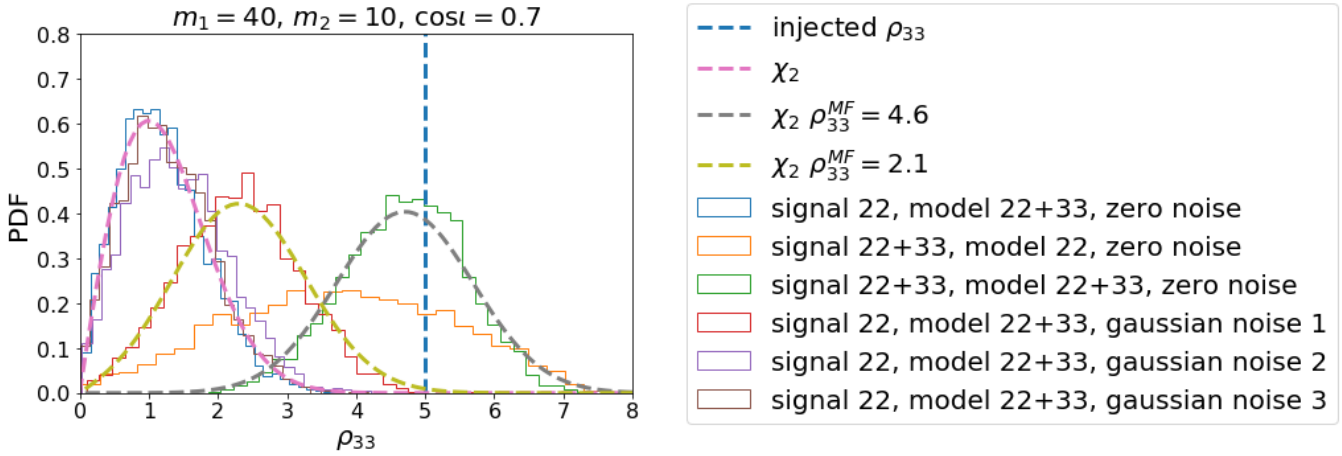

Figure 7. Posterior probability distribution for the orthogonal optimal signal-to-noise ratio of the 33 multipole. The injected parameters are $m1 = 40$, $m2 = 10$ at $\cos\iota = 0.7$.

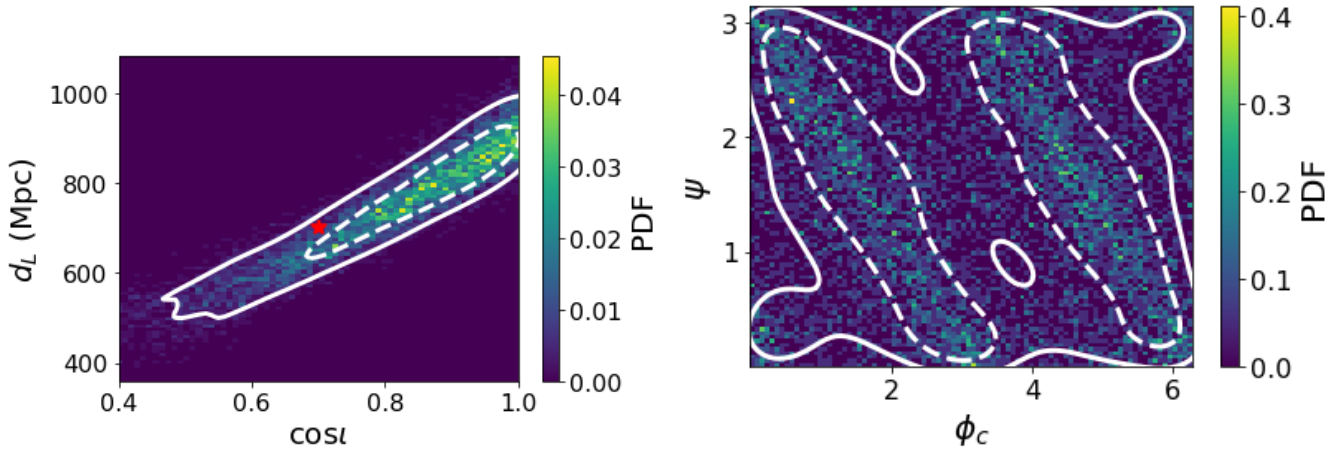

Figure 8. 2D Posterior probability distribution for *left:* inclination and distance, *right:* polarization and phase at coalescence. The injected parameters are $m1 = 40$, $m2 = 10$ at $\cos\iota = 0.7$. Templates used for parameter estimation contain only the dominant 22 multipole. The solid (dashed) lines denote 90% (50%) credible region.

$$p(\rho_{33}|s) \propto \rho_{33} \exp\left[-\frac{\rho_{33}^2 + (s|s)}{2}\right] \int_0^{2\pi} \exp\left[\rho_{33}\rho_{33}^{MF} \cos(\phi_{33} - \phi_{MF})\right] d\phi_{33} \quad (25)$$

$$\propto \rho_{33} \exp\left[-\frac{\rho_{33}^2 + (\rho_{33}^{MF})^2}{2}\right] I_0(\rho_{33}\rho_{33}^{MF}) \quad (26)$$

Where I_0 is the modified Bessel function of the first kind, and we have used the fact that $(s|s) = (\rho_{33}^{MF})^2 +$ const. [3] We recognize Eq 26 as the non-central chi distribution with 2 degrees of freedom and non-centrality parameter equal to ρ_{33}^{MF}. In the absence of a gravitational-wave signal $s = n$ where n is guassian noise. In this case, the probability distributions for the filters $(s|h_0^{33})$ and $(s|h_{\frac{\pi}{2}}^{33})$ are zero-mean, unit-variance gaussians and ρ_{33}^{MF} is chi-distributed with 2 degrees of freedom.

Finally we can interpret the distributions for $\rho_{33}^{\perp}$ under the no 33 signal hypothesis (the blue, red, purple and brown histograms in Fig. 7). The zero noise realization has ρ_{33}^{MF} by definition, so reduces to the chi-distribution. While the noise realizations 2 and 3 are consistent with a small amount of noise in the ρ_{33}^{MF} and so closely resemble the zero noise case. While the first noise realization has an excess of noise corresponding to $\rho_{33}^{MF} \sim 2.1$. We expect gaussian noise to produce $\rho_{33}^{MF} > 2.1$ in 10% of realizations.

5. DISCUSSION

In this paper, we have explored the relative significance of the higher gravitational wave harmonics in binary merger signals. For simplicity, we have decomposed the harmonics into an overall amplitude, dependent only upon the masses and spins of the system, and an orientation-dependent term, which is dependent upon the inclination and polarization but not the masses or spins. This allows us to easily identify the most significant modes, and the regions of parameter space where they are most likely to be observable. As is well known, the higher harmonics are most important when the binary is close to edge on and, indeed, we show that this maximal amplitude is corresponds to the most likely orientation, even taking into account selection effects. In addition, we show that for much of the binary parameter space, the 33 mode will be the most significant sub-dominant harmonic, with an amplitude about one quarter of the 22 mode for a mass-ratio 2 binary (over a broad range of masses). The 44 mode becomes more significant at higher masses and, although the relative amplitude is less than 0.2 for much of the parameter space, it is still the most significant sub-dominant harmonic for high-mass systems where the two components have comparable masses

For signals which are close to threshold, it is likely that only one additional mode will be clearly observable. Thus, for simplicity, we have introduced and observability criterion for the second harmonic. In many cases, the amplitude and phase of the second harmonic is largely unconstrained by the observation of the 22 mode — there are often large degeneracies in the measurement of the distance and inclination of the binary Usman et al. (2019), which lead to a broad uncertainty in the expected amplitude of the higher mode, and in the polarization and phase, which leads to a lack of knowledge of the phase of the higher modes. Consequently, the power in the second most significant mode will be χ^2 distributed with two degrees of freedom (corresponding to the unknown amplitude and phase of the mode). If there is no power in the mode, then the observed power is expected to be (centrally) χ^2 distributed while if there is power in the mode the distribution will be non-central χ^2, where the non-centrality is given by the SNR in the higher mode. We have performed a series of simulations that demonstrate this expectation is valid. Using this simple observation allows us to introduce a simple test for power in a higher mode: if the observed SNR in the mode is above 2.1, then this is unlikely to occur due to noise alone so there is evidence of a higher mode signal.

We note that this simple criterion can also be used to identify which signals, observed in a search which uses only the dominant harmonic, are likely to contain significant power in the higher harmonic. Based upon the recovered parameters, we can straightforwardly calculate the expected power in the higher modes and test whether we expect an SNR greater than 2.1 in any mode. If so, then performing parameter estimation with a higher-mode waveform will likely lead to either the observation of the higher mode, and consequent reduction in measurement uncertainty of the binary parameters, or the restriction of these parameters to regions of the parameter space where the higher harmonic amplitudes are low.

While the method introduced here is straightforward, there are several clear limitations. Most obviously, the discussion here has limited attention to a single observable harmonic. In many cases, this will be a reasonable approximation as there will be one harmonic which is is significantly larger than the others (as can be seen from the figures). Furthermore, it is likely that the observation of a single higher harmonic will be sufficient to significantly improve the ability to recover the parameters of the system, most importantly the binary orientation. The observation of additional modes will likely provide additional improvements, but possibly not the step-change of observing the second harmonic. For a detailed understanding of the impact of all of the higher harmonics, a full, Bayesian parameter estimation exploration of the issue will be necessary Kalaghatgi et al. (2019). Finally, throughout, we have restricted attention to non-precessing systems. In a recent paper, a similar analysis to the one presented here was performed on precessing systems, again with a focus on the observability of

[3] Since s is composed of components parallel, and perpindicular to the two filters h_0^{33} and $h_{\frac{\pi}{2}}^{33}$, we can always say $(s|s) = (s|h_0^{33}) + (s|h_{\frac{\pi}{2}}^{33})+$ other constant terms since we only filter once.

the two dominant harmonics Fairhurst et al. (2019b,a). For systems where both higher harmonics and precession have an observable impact on the waveform, it will be necessary to combine these ideas, to see whether it is possible to identify both the leading order precession and higher harmonic contributions to the waveform.

APPENDIX

SPIN-WEIGHTED SPHERICAL HARMONIC POLARIZATIONS

The general form for the spin-weighted spherical harmonics is

$$ {}_sY_{lm}(\iota,\phi_c) = (-1)^m \sqrt{\frac{(l+m)!(l-m)!(2l+1)}{4\pi(l+s)!(l-s)!}} \sin^{2l}\left(\frac{\iota}{2}\right) \times \sum_{r=0}^{l-s} \binom{l-s}{r} \binom{l+s}{r+s-m} (-1)^{l-r-s} e^{im\phi_c} \cot^{2r+s-m}\left(\frac{\iota}{2}\right), \tag{A1}$$

which can be written in terms of the wigner d-functions $d^{lm}_{-s}(\iota)$ (implicitly defined here)

$$ {}_sY_{lm}(\iota,\phi_c) = \sqrt{\frac{(2l+1)}{4\pi}} d^{lm}_{-s}(\iota) e^{im\phi_c}. \tag{A2}$$

They have the following symmetries

$$ {}_s\bar{Y}_{lm} = (-1)^{s+m} \, {}_{-s}Y_{l(-m)} \tag{A3}$$

$$ {}_sY_{lm}(\pi-\iota,\phi_c+\pi) = (-1)^l \, {}_{-s}Y_{lm}(\iota,\phi_c). \tag{A4}$$

The spin-weighted spherical harmonics for the modes we are interested in are

$$ {}_{-2}Y_{22} = \frac{1}{2}\sqrt{\frac{5}{\pi}} e^{2i\phi_c} \cos^4\left(\frac{\iota}{2}\right) \tag{A5}$$

$$ {}_{-2}Y_{2-2} = \frac{1}{2}\sqrt{\frac{5}{\pi}} e^{-2i\phi_c} \sin^4\left(\frac{\iota}{2}\right) \tag{A6}$$

$$ {}_{-2}Y_{21} = \frac{1}{2}\sqrt{\frac{5}{\pi}} e^{i\phi_c} \cos^2\left(\frac{\iota}{2}\right) \sin(\iota) \tag{A7}$$

$$ {}_{-2}Y_{2-1} = \frac{1}{2}\sqrt{\frac{5}{\pi}} e^{-i\phi_c} \sin^2\left(\frac{\iota}{2}\right) \sin(\iota) \tag{A8}$$

$$ {}_{-2}Y_{33} = \frac{1}{2}\sqrt{\frac{21}{2\pi}} \left(-e^{i3\phi_c)}\right) \cos^4\left(\frac{\iota}{2}\right) \sin(\iota) \tag{A9}$$

$$ {}_{-2}Y_{3-3} = \frac{1}{2}\sqrt{\frac{21}{2\pi}} e^{-i3\phi_c} \sin^4\left(\frac{\iota}{2}\right) \sin(\iota) \tag{A10}$$

$$ {}_{-2}Y_{44} = \frac{3}{4}\sqrt{\frac{7}{\pi}} e^{4i\phi_c} \cos^4\left(\frac{\iota}{2}\right) \sin^2(\iota) \tag{A11}$$

$$ {}_{-2}Y_{4-4} = \frac{3}{4}\sqrt{\frac{7}{\pi}} e^{-4i\phi_c} \sin^4\left(\frac{\iota}{2}\right) \sin^2(\iota) \tag{A12}$$

Three properties of h_{lm} help to simplify Eq (3). Firstly, specializing to planar (i.e. non-precessing) binaries allows us to write $h_{l-m} = (-1)^l h^*_{lm}$ Blanchet (2014). Secondly, in the frequency domain, $\widetilde{h^*_{lm}}(f) = \widetilde{h_{lm}}(-f)^*$. To see this, let $x(t) \equiv h_{lm}(t)$ be some complex function with r eal and imaginary parts x_r and x_I: $x(t) = x_R(t) + ix_I(t)$. Then

$$ \widetilde{x}(f) = FT[x(t)] = \int dt x(t) e^{-ift} \tag{A13}$$

$$ = \int dt \left[x_R + ix_I\right] \left[\cos ft - i \sin ft\right] \tag{A14}$$

$$ = \int dt \left[x_R \cos ft + x_I \sin ft + i(x_I \cos ft - x_R \sin ft)\right] \tag{A15}$$

$$ \widetilde{x}(-f) = \int dt \left[x_R \cos ft - x_I \sin ft + i(x_I \cos ft + x_R \sin ft)\right] \tag{A16}$$

$$ \widetilde{x}(-f)^* = \int dt \left[x_R \cos ft - x_I \sin ft - i(x_I \cos ft + x_R \sin ft)\right] \tag{A17}$$

and

$$\widetilde{x^*}(f) = FT[x^*(t)] = \int dt\,[x_R - ix_I]\,[\cos ft - i\sin ft] \tag{A18}$$

$$= \int dt\,[x_R \cos ft - x_I \sin ft - i(x_I \cos ft + x_R \sin ft)] \tag{A19}$$

$$= \widetilde{x}(-f)^* \tag{A20}$$

Finally we make the further approximation Marsat & Baker (2018) that if we only care about the waveform in direction $\hat{n}$ we can neglect one side of the frequency spectrum, depending on the sign of m. This approximation is valid in particular where the stationary phase approximation has been used Marsat & Baker (2018). We therefore assume

$$\widetilde{h_{lm}}(f) \simeq 0 \begin{cases} f > 0, m < 0 \\ f < 0, m > 0. \end{cases} \tag{A21}$$

With these three properties we can obtain explicit expressions for the orientation dependence of each of the modes

$$h_+ = \frac{1}{2}\sum_{l\geq 2}\sum_{m=-l}^{l}\left[{}_{-2}Y_{lm}(\iota,\phi_c)h_{lm} + {}_{-2}Y^*_{lm}(\iota,\phi_c)h^*_{lm}\right] \tag{A22}$$

$$\widetilde{h_+}(f) = \frac{1}{2}\sum_{l\geq 2}\sum_{m=-l}^{l}\left[{}_{-2}Y_{lm}(\iota,\phi_c)\widetilde{h_{lm}}(f) + {}_{-2}Y^*_{lm}(\iota,\phi_c)\widetilde{h_{lm}}(-f)^*\right] \tag{A23}$$

$$= \frac{1}{2}\sum_{l\geq 2}\sum_{m=1}^{l}\left[{}_{-2}Y_{lm}(\iota,\phi_c)\widetilde{h_{lm}}(f) + {}_{-2}Y^*_{l-m}(\iota,\phi_c)\widetilde{h_{l-m}}(f)^*\right] \tag{A24}$$

$$= \frac{1}{2}\sum_{l\geq 2}\sum_{m=1}^{l}\left[{}_{-2}Y_{lm}(\iota,\phi_c)\widetilde{h_{lm}}(f) + {}_{-2}Y^*_{l-m}(\iota,\phi_c)(-1)^l\widetilde{h_{lm}}(f)\right] \tag{A25}$$

$$= \frac{1}{2}\sum_{l\geq 2}\sum_{m=1}^{l}\left[{}_{-2}Y_{lm}(\iota,\phi_c) + (-1)^l\,{}_{-2}Y^*_{l-m}(\iota,\phi_c)\right]\widetilde{h_{lm}}(f) \tag{A26}$$

and similarly we can show

$$h_\times = \frac{i}{2}\sum_{l\geq 2}\sum_{m=-l}^{l}\left[{}_{-2}Y_{lm}(\iota,\phi_c)h_{lm} - {}_{-2}Y^*_{lm}(\iota,\phi_c)h^*_{lm}\right] \tag{A27}$$

$$\widetilde{h_\times}(f) = \frac{i}{2}\sum_{l\geq 2}\sum_{m=-l}^{l}\left[{}_{-2}Y_{lm}(\iota,\phi_c)\widetilde{h_{lm}}(f) + {}_{-2}Y^*_{lm}(\iota,\phi_c)\widetilde{h_{lm}}(-f)^*\right] \tag{A28}$$

$$= \frac{i}{2}\sum_{l\geq 2}\sum_{m=1}^{l}\left[{}_{-2}Y_{lm}(\iota,\phi_c) - (-1)^l\,{}_{-2}Y^*_{l-m}(\iota,\phi_c)\right]\widetilde{h_{lm}}(f) \tag{A29}$$

PSDS USED

In figure 9 we show the power spectral density of the detector noise for the O3 noise curve used in the studies in the body of the paper. For reference, we also show the PSD for aLIGO at design sensitivity and also for one proposed configuration of the Einstein Telescope (ET-D), a proposed next-generation gravitational wave observatory.

REFERENCES

Abbott, B. P., et al. 2016, Classical and Quantum Gravity, 34
Blanchet, L. 2014, Living Review Relativity, 17, 2
Cotesta, R., Buonanno, A., Boh, A., et al. 2018, Phys. Rev. D, 98, 084028
Cotesta, R., Marsat, S., & Pürrer, M. 2020, 2003.12079
Fairhurst, S., Green, R., Hannam, M., & Hoy, C. 2019a, arXiv e-prints, 1908.00555
Fairhurst, S., Green, R., Hoy, C., Hannam, M., & Muir, A. 2019b, arXiv e-prints, 1908.05707
Garca-Quirs, C., Colleoni, M., Husa, S., et al. 2020, arXiv e-prints, 2001.10914
Harry, I., Caldern Bustillo, J., & Nitz, A. 2018, Phys. Rev. D, 97, 023004
Harry, I. W., & Fairhurst, S. 2011, Phys. Rev. D, 83, 084002
Kalaghatgi, C., Hannam, M., & Raymond, V. 2019, arXiv e-prints, 1909.10010
Khan, S., Chatziioannou, K., Hannam, M., & Ohme, F. 2019, Phys. Rev. D, 100, 024059
Khan, S., Ohme, F., Chatziioannou, K., & Hannam, M. 2020, Phys. Rev. D, 101, 024056
Klimenko, S., Mohanty, S., Rakhmanov, M., & Mitselmakher, G. 2005, Phys. Rev. D, 72, 122002
Kumar Mehta, A., Tiwari, P., Johnson-McDaniel, N. K., et al. 2019, Phys. Rev. D, 100, 024032
London, L., Khan, S., Fauchon-Jones, E., et al. 2018, Phys. Rev. Lett., 120, 161102
Madau, P., & Dickinson, M. 2014, ARA&A, 52, 415
Marsat, S., & Baker, J. G. 2018, arXiv:1806.10734
Mehta, A. K., Mishra, C. K., Varma, V., & Ajith, P. 2017, Phys. Rev. D, 96, 124010

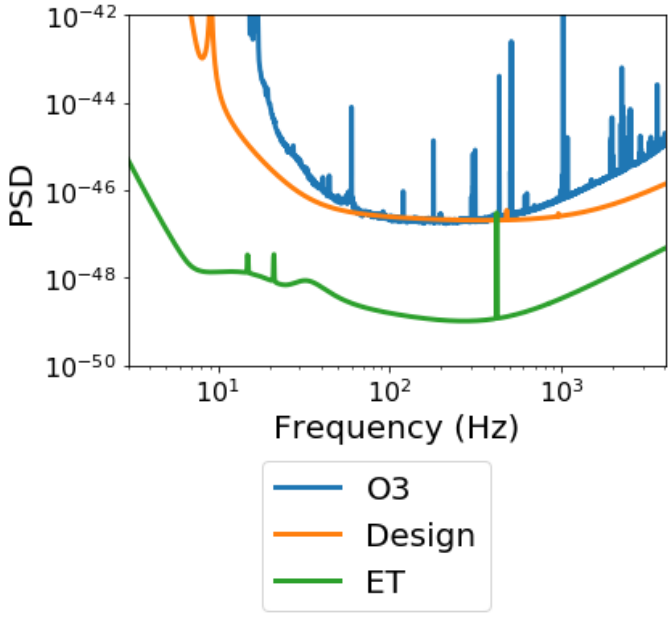

Figure 9. Power spectral density curves used in this study.

Mills, J. C., & Fairhurst, S. 2020, Supplementary Material: Measuring gravitational-wave subdominant multipoles, Tech. Rep. LIGO-P2000136
Mishra, C. K., Kela, A., Arun, K. G., & Faye, G. 2016, Phys. Rev. D, 93, 084054
Nagar, A., Riemenschneider, G., Pratten, G., Rettegno, P., & Messina, F. 2020, arXiv e-prints, 2001.09082
Ossokine, S., Buonanno, A., Marsat, S., et al. 2020, Multipolar Effective-One-Body Waveforms for Precessing Binary Black Holes: Construction and Validation, Tech. Rep. LIGO-P2000140
Rifat, N. E. M., Field, S. E., Khanna, G., & Varma, V. 2019, arXiv e-prints, 1910.10473
Schutz, B. F. 2011, Class. Quant. Grav., 28, 125023
Usman, S. A., Mills, J. C., & Fairhurst, S. 2019, Astrophys. J., 877, 82
Varma, V., Field, S. E., Scheel, M. A., et al. 2019a, Phys. Rev. Research., 1, 033015
—. 2019b, Phys. Rev. D, 99, 064045
Veitch, J., et al. 2015, Phys. Rev. D, 91, 042003